Chan Kwon Jeong
Dockwise USA,
16340 Park Ten Place, Suite 200,
Houston, TX 77084
e-mail: chankwon.jeong@gmail.com

Vijay Panchang
Maritime Systems Engineering Department,
Texas A&M University,
200 Seawolf Parkway,
Galveston, TX 77553
e-mail: panchanv@tamug.edu

Zeki Demirbilek[1]
U.S. Army Engineer Research and
Development Center,
Coastal and Hydraulics Laboratory,
3909 Halls Ferry Road,
Vicksburg, MS 39180-6199
e-mail: zeki.demirbilek@usace.army.mil

Parametric Adjustments to the Rankine Vortex Wind Model for Gulf of Mexico Hurricanes

Parametric wind models are often used to reconstruct hurricane wind fields from a limited set of hurricane parameters. Application of the Rankine Vortex and other models used in forecasting Gulf of Mexico hurricanes show considerable differences between the resulting wind speeds and data. The differences are used to guide the development of adjustment factors to improve the wind fields resulting from the Rankine Vortex model. The corrected model shows a significant improvement in the shape, size, and wind speed contours for 14 out of 17 hurricanes examined. The effect on wave fields resulting from the original and modified wind fields are on the order of 4 m, which is important for the estimation of extreme wave statistics. [DOI: 10.1115/1.4006148]

1 Introduction

In the Gulf of Mexico (GOM), extreme wave height estimates used until recently for the design of offshore structures were provided by the API [1,2]. The recommended 100-yr design significant wave height (SWH) has been, until 1990, of the order of 11 m. Comparable estimates of the 100-yr conditions were obtained by Palao et al. [3] and Panchang et al. [4], who have reported considerable spatial variability in these estimates. However, these estimates have been exceeded since 2004 by several meters. Notable examples include Hurricanes Ivan, Katrina, and Rita where SWHs exceeding 16 m were recorded at various locations (e.g., Jeong and Panchang [5]; Panchang and Li [6]). At other locations, smaller SWHs were recorded, but they still exceeded the 100-year estimates by several meters. As a result, it has become necessary to reassess the extreme wave climatology in the GOM region (e.g., Berek et al. [7]). Similar efforts are underway to reassess extreme storm surge and coastal inundation effects in this region.

The U.S. Army Corps of Engineers, Geological Survey, and National Oceanic and Atmospheric Administration (NOAA) are developing methods to predict the coastal impacts of extreme storms on the coasts of the United States. The primary emphasis in these studies is on the numerical modeling of hurricanes (https://ipet.wes.army.mil/) and typhoons [8–12], whereas Demirbilek et al. [13] and Demirbilek and Nwogu [14] focused on modeling the effects of highly nonlinear storm waves on fringing reefs. These efforts are directed towards predicting where maximum coastal erosion will occur, where storm surge and waves will overtop beaches, where sand dunes will retreat landward, and where breaches will sever barrier islands and create new inlets. For example, during Hurricane Katrina, the surge level in Lake Pontchartrain was roughly the same as the design levels assumed for the Hurricane Protection System. On the east side of New Orleans, Katrina-generated surges were significantly greater than the design criteria, ranging from 5.2 to 6.1 m compared to the 3.7 to 4.3 m assumed in the design. Typically, these types of studies require the development of historical wind fields, which can then be used for developing design criteria for offshore structures and coastal protection systems such as levees.

In the GOM, wind/wave data can be obtained from NDBC buoys which provide data for a maximum duration of approximately 35 years. These data provide "spot measurements" and at other locations one must resort to numerical modeling to obtain the correct spatial variability in the wind (and in the resulting wave and storm surge) estimates. For numerical modeling purposes, four types of wind fields (on different spatial and temporal grids) are available:

(1) Using the most sophisticated models available, the National Center for Environmental Prediction (NCEP) produces wind fields on an ongoing basis every 6 h. In the GOM, the simulations are made using their "Western North Atlantic" and "North Atlantic Hurricane" models, and wind fields are available on a $0.25° \times 0.25°$ grids. These simulations represent the estimates of the entire GOM wind fields; however, they are not available prior to 1999. Thus, alternative methods must be explored if hindcasts for that period are needed.

(2) The NCEP and the National Center for Atmospheric Research have developed the "Reanalysis" wind field dataset, using a combination of mathematical models and data assimilation (Kalnay et al. [15]). An example is shown in Fig. 1 (left) for Hurricane Gordon. These wind fields are available for the period starting at 1948 at a temporal resolution of 6 h; however the spatial resolution is coarse ($2.5° \times 2.5°$). As a result, some features of a hurricane may not be well represented by these data, despite their use in large areas such as the Atlantic [16–20].

(3) A dataset representing hurricane measurements since 1995 has been developed by the National Hurricane Center [21,22]. This dataset, called H*Wind, is available for the post-1994 period, and has been widely used by researchers for various applications (e.g., Kennedy et al. [23]; Powell et al. [24]). It is an estimate of the wind field based on available observations, viz., aircraft-based, land-based, sea-based, and satellite-based. Based on a standardization technique to process data from diverse sources, it provides wind fields at a resolution of approximately 6 km (an example is shown in Fig. 1). As may be expected, however, this dataset is not continuous (except in the recent past), does not cover all hurricanes, exhibits a spatial range limited to the immediate vicinity of the hurricane, and is available at irregular time steps.

(4) A dataset pertaining to a limited set of storm parameters has been developed by the NOAA for a period going back to the second half of the 19th century. This dataset, called HURDAT, provides, at 6 h intervals, information such as the location of the storm center (LatC, LonC), storm direction (θ_s), storm speed (V_s), maximum wind speed (V_m), and

---

Report Documentation Page		*Form Approved* *OMB No. 0704-0188*

Public reporting burden for the collection of information is estimated to average 1 hour per response, including the time for reviewing instructions, searching existing data sources, gathering and maintaining the data needed, and completing and reviewing the collection of information. Send comments regarding this burden estimate or any other aspect of this collection of information, including suggestions for reducing this burden, to Washington Headquarters Services, Directorate for Information Operations and Reports, 1215 Jefferson Davis Highway, Suite 1204, Arlington VA 22202-4302. Respondents should be aware that notwithstanding any other provision of law, no person shall be subject to a penalty for failing to comply with a collection of information if it does not display a currently valid OMB control number.

1. REPORT DATE **NOV 2012**	2. REPORT TYPE	3. DATES COVERED **00-00-2012 to 00-00-2012**
4. TITLE AND SUBTITLE **Parametric Adjustments to the Rankine Vortex Wind Model for Gulf of Mexico Hurricanes**		5a. CONTRACT NUMBER
		5b. GRANT NUMBER
		5c. PROGRAM ELEMENT NUMBER
6. AUTHOR(S)		5d. PROJECT NUMBER
		5e. TASK NUMBER
		5f. WORK UNIT NUMBER
7. PERFORMING ORGANIZATION NAME(S) AND ADDRESS(ES) **U.S. Army Engineer Research and Development Center,Coastal and Hydraulics Laboratory,3909 Halls Ferry Road,Vicksburg,MS,39180**		8. PERFORMING ORGANIZATION REPORT NUMBER
9. SPONSORING/MONITORING AGENCY NAME(S) AND ADDRESS(ES)		10. SPONSOR/MONITOR'S ACRONYM(S)
		11. SPONSOR/MONITOR'S REPORT NUMBER(S)

12. DISTRIBUTION/AVAILABILITY STATEMENT **Approved for public release; distribution unlimited**

13. SUPPLEMENTARY NOTES

14. ABSTRACT

15. SUBJECT TERMS

16. SECURITY CLASSIFICATION OF:			17. LIMITATION OF ABSTRACT	18. NUMBER OF PAGES	19a. NAME OF RESPONSIBLE PERSON
a. REPORT **unclassified**	b. ABSTRACT **unclassified**	c. THIS PAGE **unclassified**	**Same as Report (SAR)**	**17**	

Standard Form 298 (Rev. 8-98)
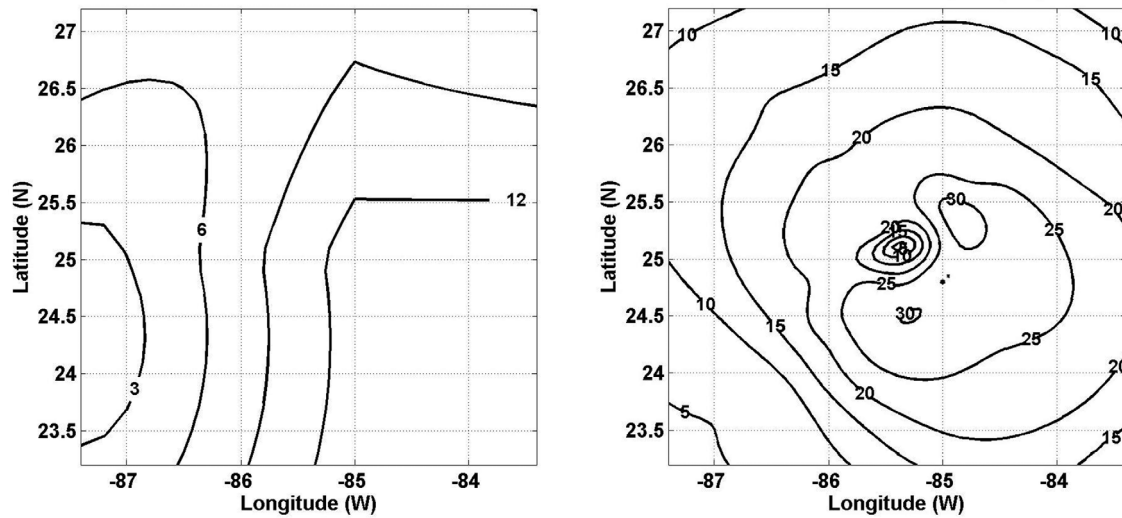Prescribed by ANSI Std Z39-18

Fig. 1   Wind-field (m/s) for Hurricane Gordon, 0000 UTC 17 Sept. 2000; Reanalysis (left), and H*Wind field (right)

storm central pressure (P_c). Obviously, these data do not provide details of a complete wind field.

For recreating historical wind fields on a continuous basis for a grid covering the entire GOM, neither the H*Wind nor the Reanalysis wind fields are completely adequate. Planetary boundary layer models may be used to construct spatially varying wind fields for the GOM region (e.g., Thompson and Cardone [12]), but this requires using a complicated wind model that may not be practical. Therefore, here we have taken the approach of developing wind fields using parametric formulations that depend on a limited set of parameters (HURDAT). This approach has been used, for instance, by Phadke et al. [25] and Sanchez et al. [9,10], for simulating tropical cyclones near Hawaii, and by McAfee and Pearson [26] for simulating mid-Atlantic hurricanes. Additionally, extensions to real-time surface wind forecasting using such models is possible (Xie at al. [27]).

A summary of five parametric models is given by MacAfee and Pearson [26]. These are the Rankine Vortex (RV) model [25], the SLOSH model [28], the Holland model [29], the vortex simulation model [30], and the Willoughby and Rahn model [31]. Sanchez et al. [9,10] have used variations of these parameteric models in their studies of typhoon-induced flooding and inundation of the Pacific Islands by tropical storms, and provided corrections for asymmetric wind patterns and options for the parameterization of storm characteristics. In addition, Emanuel et al. [32] describe an alternative model with a structural form similar to the parametric vortex developed by Holland [29]. In general, these parametric models provide the wind speed $V(x, y)$ as a function of hurricane parameters V_m and P_c, maximum hurricane wind speed and central pressure, and also other model-calculated quantities such as the radius to maximum wind (R_m), sea level pressure at the last closed isobar (P_n), etc. (Note that all numerical models do not include all these parameters.) As an example, for Hurricane Katrina, HURDAT provides the parameters noted at the bottom of this page.

These parameters, in combination with various parametric models, result in the wind field plots shown in Fig. 2 (left). Typically, the basic models yield a symmetric pattern and asymmetry may

also be parametrically introduced [33], which leads to the plots shown in Fig. 2 (right).

There is, of course, no consensus on which model should be used; nor is it reasonable to expect any one model to faithfully reproduce every hurricane. Researchers have had to make adjustments to suit individual cases or locations, as is noted later. For the purpose of recreating historical wind fields in the GOM, here we focus on the RV model (described in Sec. 2). This choice is based on the conclusions of Phadke et al. [25] who found that the first three models produced the same results in the core of the hurricane, however, the RV model had better overall agreement with data outside the core. The performance of this model is examined against data pertaining to five recent hurricanes in Sec. 2. The observed discrepancies are used to make adjustments to the RV model; these are described in Sec. 3. In Sec. 4, the performance of the adjusted model is examined using wind data from twelve other hurricanes. The effect of the modified wind fields on wave simulation is also demonstrated.

2   The RV Model and its Application to Recent Hurricanes

The RV model provides a radially symmetric hurricane wind field as follows

$$V = \begin{cases} V_m\left(\dfrac{R}{R_m}\right)^B, & R < R_m \\[2mm] V_m\left(\dfrac{R_m}{R}\right)^B, & R \geq R_m \end{cases} \tag{1}$$

where V_m is the maximum wind speed, R is the radial distance from the storm center, R_m is the radius to maximum winds, and B is a shape parameter (≈ 0.5). The radius to maximum winds (R_m in km) has been described by MacAfee and Pearson [26] as a function of the latitude (φ in degrees), the central pressure (mb), and the pressure along the last closed isobar (P_n in mb) as follows

$$1nR_m = 2.636 - 0.00005086(P_n - P_c)^2 + 0.0394899\varphi \tag{2}$$

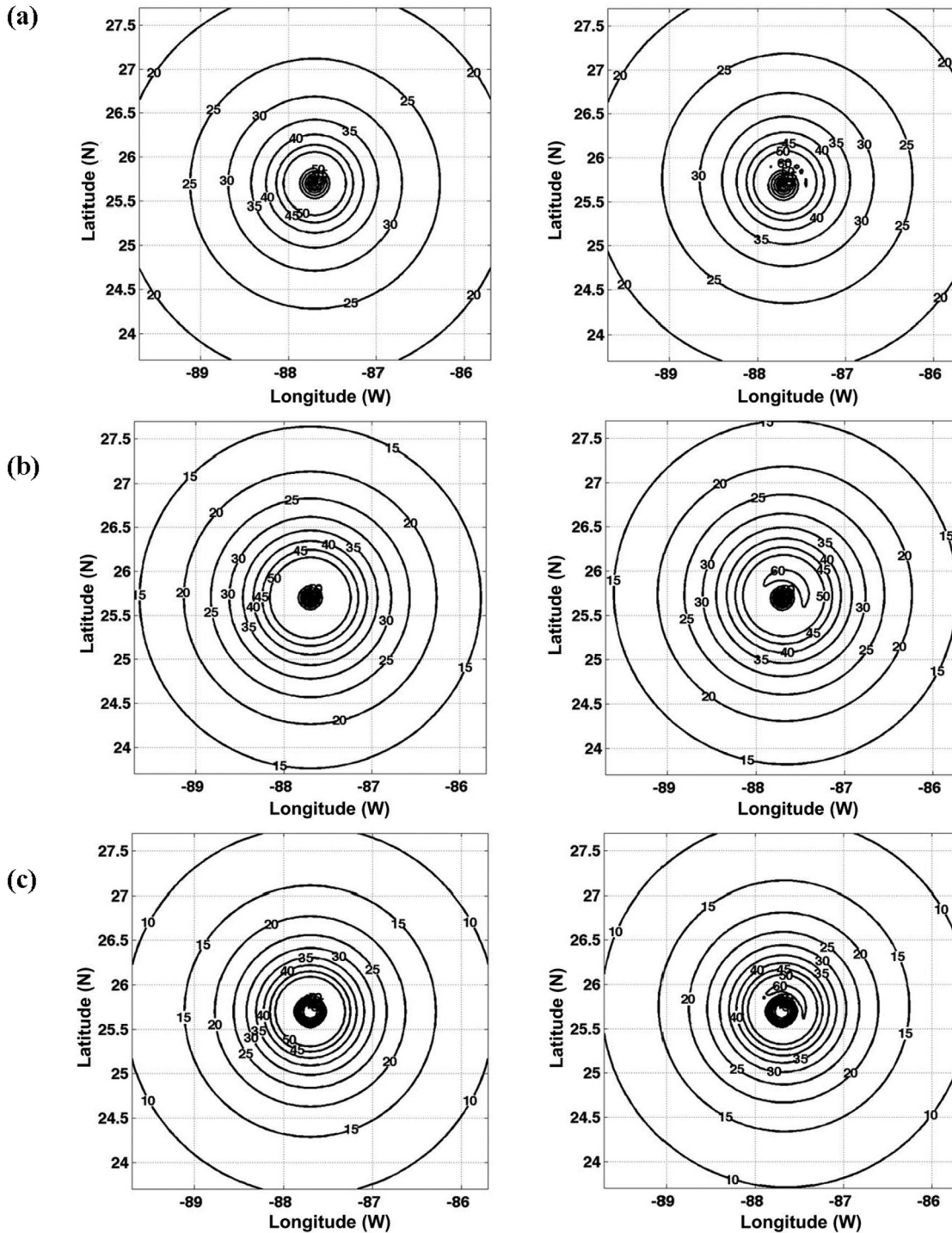| Month	Day	Hour	LatC	LogC	Dir. (θ_r)	Translational speed:V_s (km/h)	Max wind speed: V_m (km/h)	Pressure: P_c (mb)	Type
						−			
						−			
8	28	12	25.7	87.7	300	18	270	909	Category 5
						−			

Fig. 2 Symmetric (left) and asymmetric (right) wind speeds (m/s) during Hurricane Katrina (1200 UTC 28 Aug. 2005); (*a*) Rankine Vortex model, (*b*) SLOSH model, and (*c*) Holland model

where

$$P_n = P_c - 20.69 + 1.33V_m + 0.11\varphi \qquad (3)$$

Willoughby et al. [34] provide an alternative formula to estimate R_m as a function of the latitude and maximum wind speed. The importance of properly introducing asymmetry to the RV model has been emphasized by Liu et al. [35]. This can be accomplished by making an adjustment to V due to storm translation. The net motion-adjusted wind velocity may then be obtained as

$$V_{RV} = \left\{ (-V\cos\theta_r)^2 + \left[V\sin\theta_r + \frac{V_s R_m R}{(R_m^2 + R^2)} \right]^2 \right\}^{1/2} \qquad (4)$$

where θ_r is the angle between the storm direction and the radius to a particular grid point, and V is the estimated model wind speed, resulting from Eq. (1) [26]. For the wind direction, a circular wind flow pattern is assumed and a cross-isobaric direction correction β, proposed by Bretschneider [36], can be applied to each grid point

Table 1 HURDAT dataset for five hurricanes

IVAN – 2004

Month	Day	Hour	Lat.	Log.	Dir.	Translational speed (km/h)	Max wind speed (km/h)	Pressure (mb)	Type
9	13	0	19.5	82.8	300	12	260	916	Category 5
9	13	6	19.9	83.5	300	12	260	920	Category 5
9	13	12	20.4	84.1	310	12	260	915	Category 5
9	13	18	20.9	84.7	310	12	260	912	Category 5
9	14	0	21.6	85.1	330	12	260	914	Category 5
9	14	6	22.4	85.6	330	16	260	924	Category 5
9	14	12	23	86	330	12	230	930	Category 4
9	14	18	23.7	86.5	325	14	220	931	Category 4
9	15	0	24.7	87	335	18	220	928	Category 4
9	15	6	25.6	87.4	340	16	220	935	Category 4
9	15	12	26.7	87.9	340	20	215	939	Category 4
9	15	18	27.9	88.2	345	22	215	937	Category 4

KATRINA - 2005

Month	Day	Hour	Lat.	Log.	Dir.	Translational speed (km/h)	Max wind speed (km/h)	Pressure (mb)	Type
8	26	18	24.9	82.6	250	9	160	968	Category 2
8	27	0	24.6	83.3	245	12	165	959	Category 2
8	27	6	24.4	84	255	11	175	950	Category 2
8	27	12	24.4	84.7	270	11	185	942	Category 3
8	27	18	24.5	85.3	280	9	185	948	Category 3
8	28	0	24.8	85.9	300	11	185	941	Category 3
8	28	6	25.2	86.7	300	14	230	930	Category 4
8	28	12	25.7	87.7	300	18	270	909	Category 5
8	28	18	26.3	88.6	305	18	280	902	Category 5
8	29	0	27.2	89.2	330	18	260	905	Category 5
8	29	6	28.2	89.6	340	18	230	913	Category 4

RITA - 2005

Month	Day	Hour	Lat.	Log.	Dir.	Translational speed (km/h)	Max wind speed (km/h)	Pressure (mb)	Type
9	21	0	24.1	82.7	280	18	175	967	Category 2
9	21	6	24.2	84	275	20	205	955	Category 3
9	21	12	24.2	85.2	270	18	220	941	Category 4
9	21	18	24.3	86.2	275	16	270	920	Category 5
9	22	0	24.5	86.9	285	11	280	897	Category 5
9	22	6	24.8	87.6	295	12	285	897	Category 5
9	22	12	25.2	88.3	300	12	260	908	Category 5
9	22	18	25.6	89.1	300	14	230	913	Category 4
9	23	0	26	89.9	300	14	220	915	Category 4
9	23	6	26.5	90.7	305	14	215	924	Category 4
9	23	12	27.1	91.5	310	16	215	927	Category 4
9	23	18	27.8	92.3	315	16	205	930	Category 3
9	24	0	28.6	93	320	18	195	931	Category 3

DOLLY - 2008

Month	Day	Hour	Lat.	Log.	Dir.	Translational speed (km/h)	Max wind speed (km/h)	Pressure (mb)	Type
7	21	18	22.8	90.4	305	31	85	1005	Tropical Storm
7	22	0	23	92	280	25	85	1000	Tropical Storm
7	22	6	23.2	93.3	280	22	85	999	Tropical Storm
7	22	12	23.7	94.1	305	14	100	993	Tropical Storm
7	22	18	24.3	94.9	310	16	110	990	Tropical Storm
7	23	0	24.9	95.7	310	16	120	982	Category 1
7	23	6	25.4	96.2	320	11	130	982	Category 1

IKE - 2008

Month	Day	Hour	Lat.	Log.	Dir.	Translational speed (km/h)	Max wind speed (km/h)	Pressure (mb)	Type
9	10	0	23.1	84	300	12	120	968	Category 1
9	10	6	23.4	84.6	300	11	130	964	Category 1
9	10	12	23.8	85.2	305	11	150	959	Category 1

Table 1. *Continued*

IKE - 2008

Month	Day	Hour	Lat.	Log.	Dir.	Translational speed (km/h)	Max wind speed (km/h)	Pressure (mb)	Type
9	10	18	24.2	85.8	305	11	160	958	Category 2
9	11	0	24.7	86.4	310	12	160	944	Category 2
9	11	6	25.1	87.1	300	12	160	945	Category 2
9	11	12	25.5	88	295	16	160	946	Category 2
9	11	18	25.8	88.9	290	14	160	952	Category 2
9	12	0	26.1	90	285	18	160	954	Category 2
9	12	6	26.4	91.1	285	18	165	954	Category 2
9	12	12	26.9	92.2	295	20	175	954	Category 2
9	12	18	27.5	93.2	305	18	175	954	Category 2
9	13	0	28.3	94	320	18	175	952	Category 2

$$\beta = \begin{cases} 10° + \left(1 + \dfrac{R}{R_m}\right), & R < R_m \\[2mm] 20° + 25°\left(\dfrac{R}{R_m} - 1\right), & R_m \leq R < 1.2R_m \\[2mm] 25°, & R \geq 1.2R_m \end{cases} \quad (5)$$

The final wind flow is, thus, anticlockwise at a direction of $(90-\beta)$ degrees to the radius at any point.

In this study, five prominent Gulf of Mexico hurricanes that occurred during the 2004-2008 period are chosen for a detailed examination. These are Ivan (2004), Katrina (2005), Rita (2005), Dolly (2008), and Ike (2008). At the location of one or more NDBC buoys in the GOM, wave heights recorded during four of these storms were larger than those recorded prior to 2004, and in some cases exceeded the 100-yr event [5,6]. The HURDAT details of these hurricanes are provided in Table 1. As can be seen, these data provide a total of 56 snapshots. (In actuality, more snapshots are available in the HURDAT dataset, but the others extend over regions outside the GOM, including land, and hence, are not considered.) These snapshots cover the entire range of hurricane development phases/levels (e.g., from the "tropical storm" category to category 5, central pressures ranging between 902 mb and 1005 mb, and wind speeds varying between 85 km/h and 285 km/h). Additionally, these storms were chosen because they had the largest number of HURDAT snapshots for validation.

Some results of the wind fields calculated using Eqs. (1)–(5) for the set of parameters in Table 1 are shown Figs. 3(a) and 4(a). The results represent one snapshot from each of the five storms. The corresponding H*Wind datasets are shown in Figs. 3(b) and 4(b). A comparison suggests that the parametric model needs adjustment to obtain a better match with the data. In particular, for some storms the "bean shape" in the core is insufficiently developed and the distribution of the velocity contours is tighter (smaller) than the data (e.g., the plots show considerable underestimation in many areas, especially on the right side of the hurricane). Figure 5 shows the wind speed along the central East-West radial, calculated using not only the RV model (Eqs. (1)–(5)), but also the widely-used SLOSH and Holland models. All three models show a mismatch (and a similar mismatch was also seen in the N-S transect) indicating a need for adjustment. Wind speed errors are as large as 15 m/s, and when used with a wave model, the resulting errors in SWHs can be of the order of several meters, as shown in Fig. 6.

This type of mismatch has also been observed in other studies and typically, adjustments may have to be made by using data to develop alternative equations. For example, Xie et al. [27] made adjustments to the Holland model based on four mid-Atlantic hurricanes. Instead of treating R_m as independent of θ, they found it preferable to describe it as a power series of θ with the constants being determined on a case-by-case basis, for which details such as wind speeds at specific locations are required. For our work, such data are not available (especially for the pre-1994 period).

Sanchez et al. [9,10], MacAfee and Pearson [26], and Willoughby et al. [34] also made adjustments which were tailored for mid-latitude applications.

3 Adjustments to the RV Model

In order to make adjustments to the RV model, the calculated wind speed plots were compared with H*Wind plots for the five chosen hurricanes. In general, the RV-model results were frequently similar to H*Wind for strong hurricanes (e.g., for $P_c < 930$ mb). In other instances, however, both the shape and the magnitudes were incorrect. Based on the differences, correction factors $d(\theta)$ and C_B were established. The first correction factor was intended to modify the RV-modeled hurricane shape and the second was intended to modify the size and velocity distributions. The net wind field V_{CRV} is obtained in two stages, as follows

$$V_{RV1} = V_{RV} \times d(\theta)$$

$$V_{CRV} = V_{RV1} \times C_B$$

3.1 Development of Correction Factor $d(\theta)$. A detailed examination of the modeled and H*Wind plots indicated that the comparison was acceptable for lower P_c values (Fig. 7 (top)), however, for larger values of P_c the hurricane shape was more deformed relative to the modeled shape (Fig. 7 (bottom)), i.e., the hurricane was less circular in shape and developed a more pronounced bean-shaped central feature than in the model.

To accommodate these features, it was necessary to appropriately deform the modeled RV contour shapes. Since the RV model produces largely circular contours, the values of the H*Wind data velocities along any circle (after appropriate normalization) can be used as a measure of the required deformation $d(\theta)$. For example, denoting the H*Wind velocities at three arbitrary points P, Q, and B along a circle (shown in Fig. 8) by V_P, V_Q, and V_B, respectively, the ratios $d_P = V_P/V_B$ and $d_Q = V_Q/V_B$ can be used as a measure of the deviation of the contour from a circle. A circle with radius $4R_m$ is nominally selected for this purpose (to go sufficiently far from the center), and $d(\theta)$ values are estimated at selected points on the circle. These estimates are used to calculate the deformation $d(\theta)$ at other points by curve-fitting.

To be specific, the point with the smallest velocity on this circle was denoted by "C." Two other points (A and B) were located on the circle in order to create radii perpendicular to the one to C (Fig. 8 (left)). Using point B as the base velocity, the ratios $d_A = V_A/V_B$ and $d_C = V_C/V_B$ were estimated to provide measures of deformation at these points. These data are provided in Table 2 in the form of averages for each storm.

The values of d_A for the 56 plots were found to vary in a relatively small range ($\pm 4\%$) around the average, and hence, the average (≈ 1.15) was used as the deformation factor. On the contrary, the ratio d_C displayed less uniformity (varying between -16% and $+6\%$ around the average) and was found to depend on the
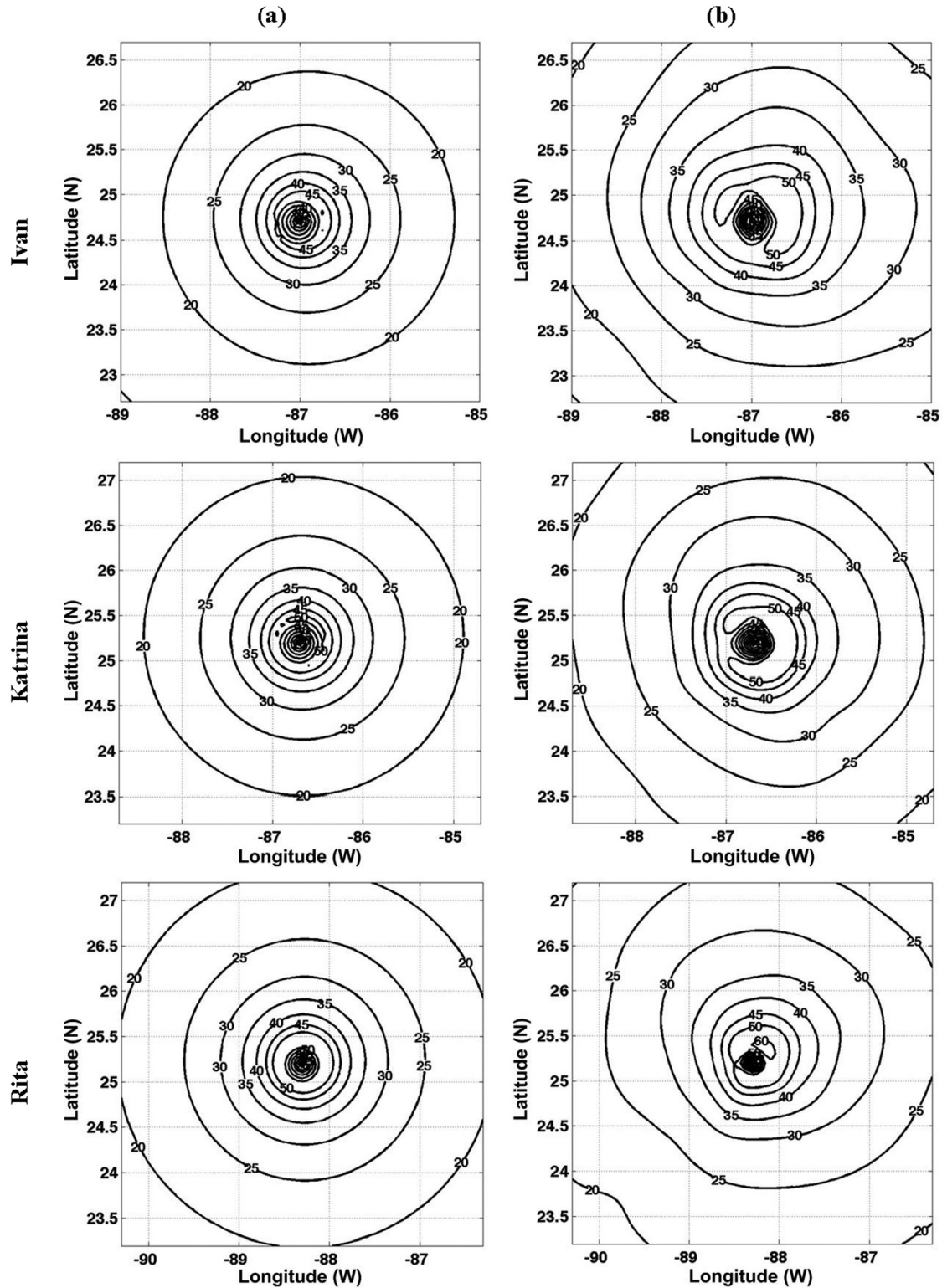
Fig. 3 Wind fields (m/s) for hurricanes Ivan, Katrina, and Rita: (*a*) asymmetric RV model, and (*b*) H*Wind

central pressure, as seen in Fig. 9. Since $930 \leq P_c \leq 970$ for most of the cases examined, a best-fit line was used to define this deformation ratio as follows

$$
\begin{aligned}
d_C &= 0.8 + 02.\alpha \text{ for } \quad 930 \leq P_c \leq 970 \\
d_C &= 1, \qquad \text{ for } \quad P_c \leq 930 \\
d_C &= 0.8, \qquad \text{ for } \quad P_c \geq 970
\end{aligned}
\tag{6}
$$

where $\alpha = (970 - P_c) / 40$.

It is now necessary to find $d(\theta)$ using the deformation at A, B, and $C(d_A, d_B,$ and $d_C)$, for which reference to Fig. 10 is made. The right curve between A and B was described by $d(\theta) = a_1\theta + b_1$, where d_A and d_B (i.e., information at $\theta = 0$ and $\theta = \pi$) are used to determine a_1 and b_1. The left half was described by $d(\theta) = a_2 \cos(2\theta) + b_2$ for $\pi < q < 3/2p$ and $d(\theta) = a_3 \cos(2\theta) + b_3$ for $3/2\pi < q < 2p$, and a_2 and b_2 are obtained from
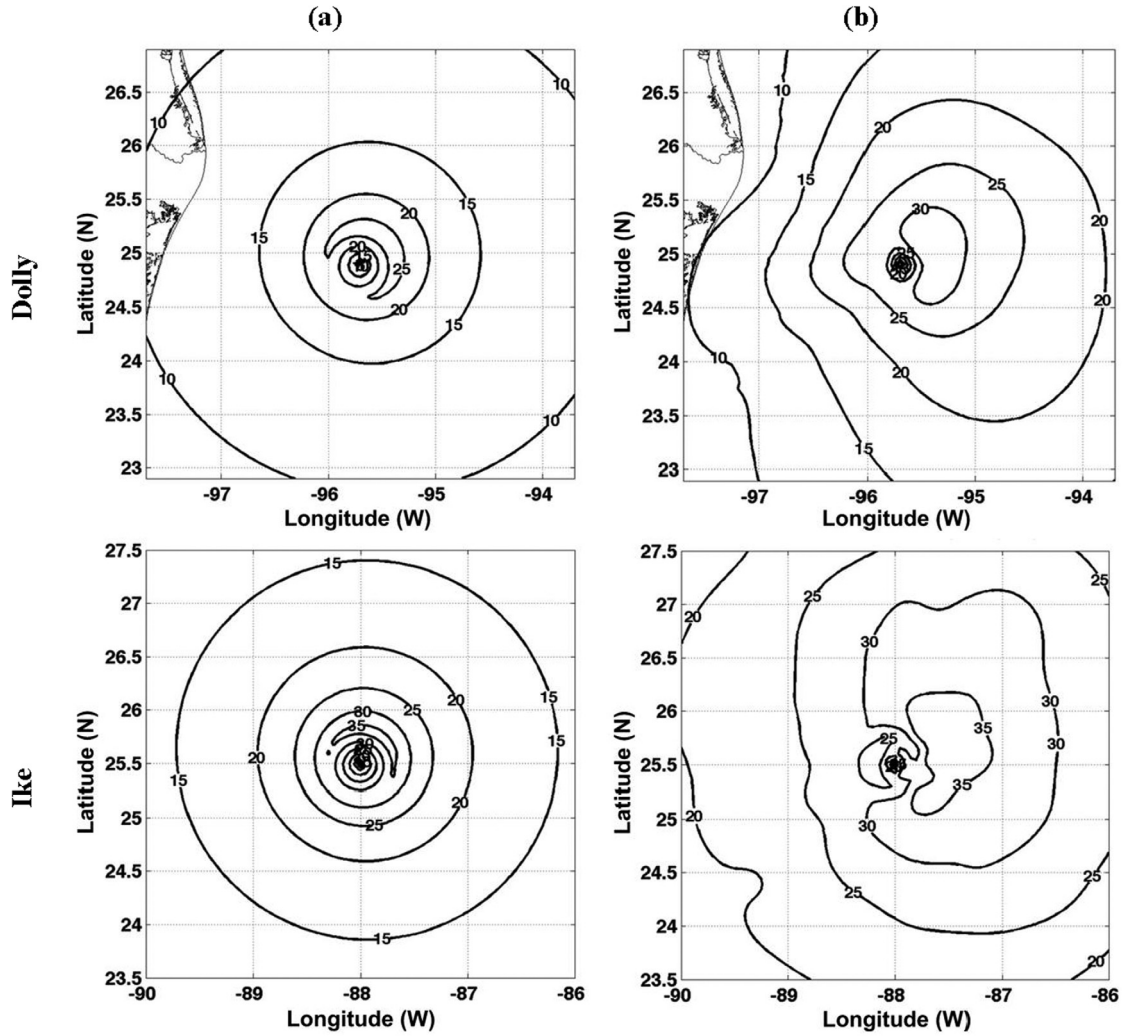
Fig. 4 Wind fields (m/s) for hurricanes Dolly and Ike: (*a*) asymmetric RV model, and (*b*) H*Wind

d_B and d_C, and a_3, b_3 are from d_C and d_A. These calculations lead to

$$d(\theta) = 1.15 - (0.15/\pi)\theta, \quad 0 < \theta \le \pi$$
$$d(\theta) = 1 - (1 - d_c)\sin^2\theta, \quad \pi < \theta \le \frac{3}{2}\pi \qquad (7)$$
$$d(\theta) = d_c + (1.15 - d_c)\cos^2\theta, \quad \frac{3}{2}\pi < \theta \le 2\pi$$

Multiplying the RV model velocities by $d(\theta)$ changes the largely circular contour shape; however, it is first necessary to determine the locations with the closest correspondence to *A*, *B*, and *C* on the modeled contours. For the parametric model, theoretically (based on Eq. (4)) the radius to point *A* is in the same direction as the storm direction. However, the data show that this is not always true. The actual storm direction can be found from the 56 H*Wind plots (see Fig. 11). Generally, strong hurricane conditions agreed with this theoretical expectation the of storm direction and radius to *A* being collinear, however, for other hurricanes the storm speed, storm direction, and central pressure affect the orientation of *A*, *B*, and *C*. Using the 56 plots we attempted to determine the angles between the radius to *A* and the storm track (θ_c). Unfortunately, no simple pattern emerged. Therefore, the data points were placed into 6 categories based on storm direction. While no meaningful difference between the two vectors was observed for

$0 < \theta < 180$, for the other sectors, the difference varied with P_c and V_s. The results are summarized in Table 3. The net θ used in Eq. (7) is, therefore, the sum of θ_r and θ_c.

Figure 12 shows plots for the wind fields pertaining to H*Wind, the RV model, the RV model with the $d(\theta)$ correction before applying the θ_c correction, and the RV model with the corrected θ. The hurricane shape in Fig. 12(*d*) is a clearly substantial improvement over the basic RV model. However, the hurricane size and the velocity distribution are not well matched; thus, further adjustment is required.

3.2 Development of Correction Factor C_B. Imperfections at any grid point in the modeled velocity V_{RV1} are due to two reasons. The first is due to the fact that the modeled velocity is not at the 10 m elevation, whereas H*Wind is; the second is due to errors in the hurricane size and velocity distributions. The first error is addressed in this paper as a function of r, and the second as a function of both r and θ. In other words, we provide a correction to the V_{RV1} using a correction factor C_B that includes both sources of errors, defined as

$$C_B(r, \theta) = f_1(r) + f_2(r, \theta) \qquad (8)$$

The function $f_1(r)$ was chosen as a constant ($\cong 0.8$) by Phadke et al. [25]. Figure 13 shows an example of the RV modeled wind and the corresponding data along the central transect for hurricane Katrina (0600 UTC, 8/27/2005), with an adjustment by a factor of
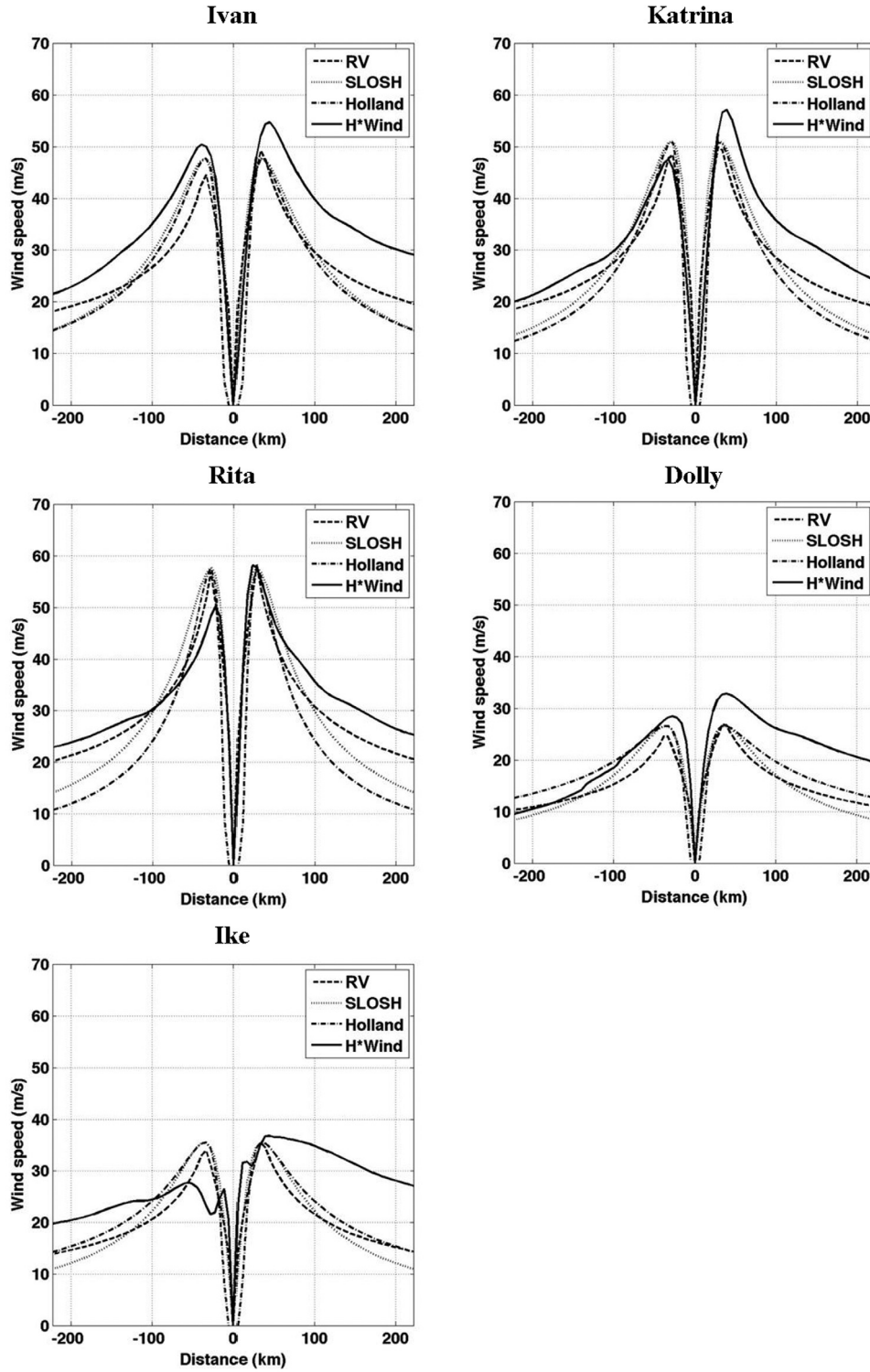
Fig. 5   Modeled and measured wind velocities along the central transect

0.8 (Fig. 13(*b*)). It is obvious that this adjustment leads to an underestimation outside the core. An examination of several such plots suggested that instead of using a constant, the following function was to be preferred

$$f_1(r) = 0.8 + 0.2\left(\frac{r - R_m}{3R_m}\right), \qquad \text{for } R_m \leq r \leq 4R_m$$

$$f_1(r) = 1, \qquad \text{for } r > 4R_m$$

$$f_1(r) = 0.8, \qquad \text{for } r < R_m$$

(9)

This leads to an improvement, as shown in Fig. 13(*c*).

As to the correction necessitated by varying storm sizes, the function $f_2(r, \theta)$ was, for simplicity, described as

$$f_2(r, \theta) = F_2(r) \cdot E(\theta) \qquad (10)$$

In order to estimate $F_2(r)$ and $E(\theta)$, the discrepancies $\Delta(r, \theta)$ between V_{RV1} and H*Wind at approximately 100 points along four radii (corresponding to $\theta = 0°$, $90°$, $180°$, and $270°$) were
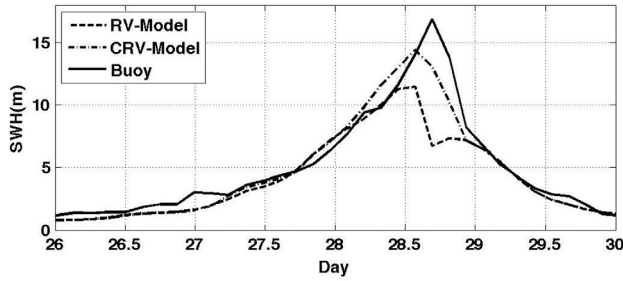
Fig. 6 SWH comparison plot during Hurricane Katrina (Aug. 2005) at NDBC buoy 42 040, located approximately 174 km from the storm track

determined. From the 400 values of $\Delta(r, \theta)$, the maximum discrepancy Δ_{max} was determined.

In general, two patterns for the discrepancies were observed, as shown in Figs. 14 and 15 (left frames), based on wind-speed

ranges. However, the similarity of the curves in the r-direction for different directions justifies the separation of variables chosen in Eq. (10). For the storms with 36 m/s $< V_m <$ 50 m/s, the maximum discrepancy for each θ, denoted by $\Delta_m(\theta)$, occurred at approximately $r = 4R_m$. Figure 14 (right) shows a composite of all discrepancies for such cases. A regression analysis was used to fit the following curve to rectify these errors

$$\frac{\Delta(r, \theta)}{\Delta_m(\theta)} = 0 \quad \text{for} \quad r < R_m$$

$$\frac{\Delta(r, \theta)}{\Delta_m(\theta)} = -0.0218r^3 + 0.1017r^2 + 0.281r - 0.3609, \quad R_m < r < 4R_m$$

(11)

$$\frac{\Delta(r, \theta)}{\Delta_m(\theta)} = -0.000333r^3 + 0.01639r^2 + 0.12041r - 0.7565,$$

$$\times 4R_m < r < 15R_m$$
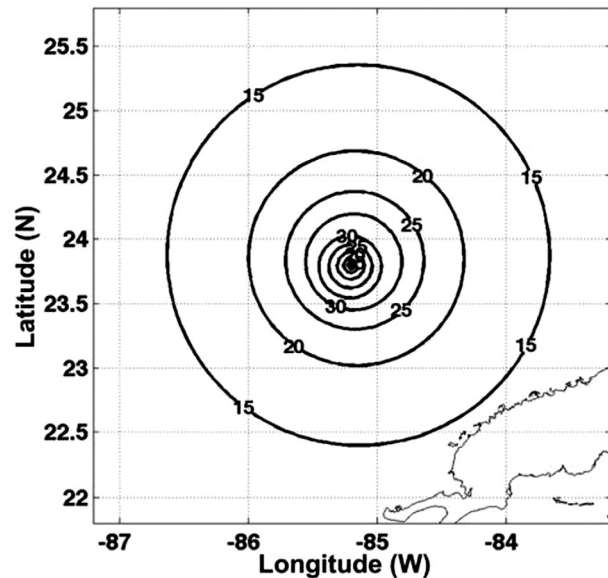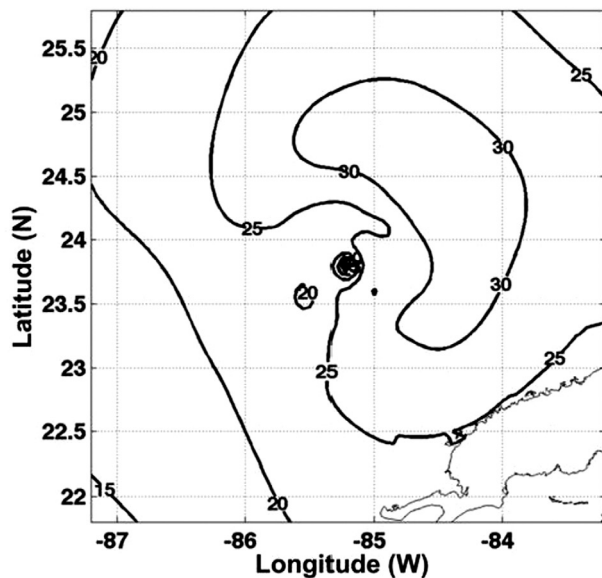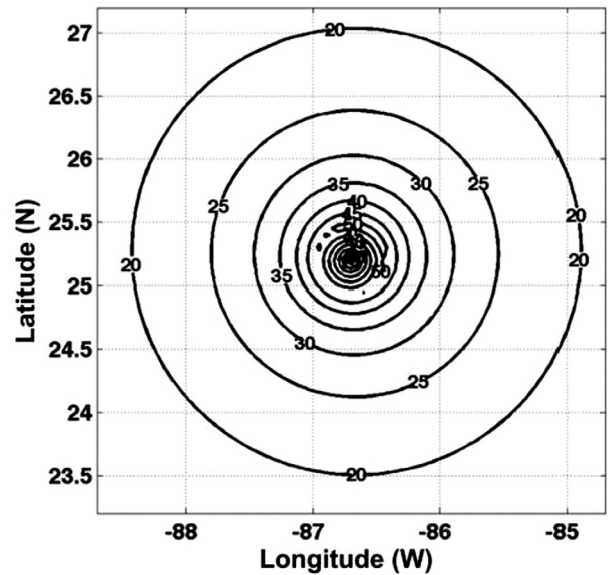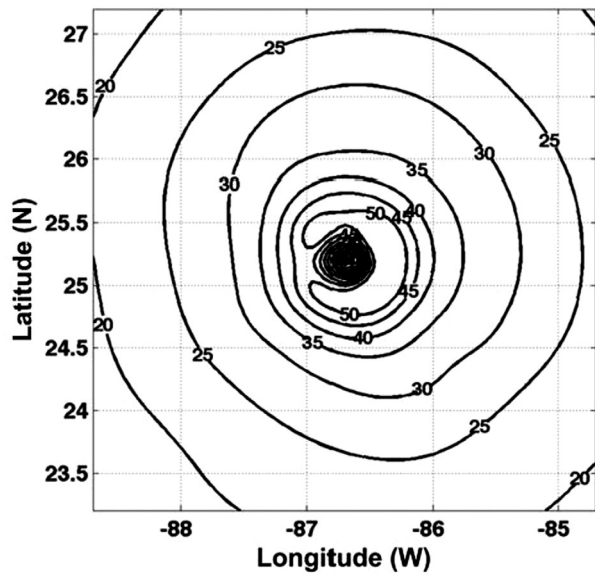
Fig. 7 H*Wind (left) and RV-model (right) wind speeds (m/s): Katrina (0600 UTC 28 August. 2005), P_c = 930 (top); Ike (1200 UTC 10 September. 2008), P_c = 959 (bottom)
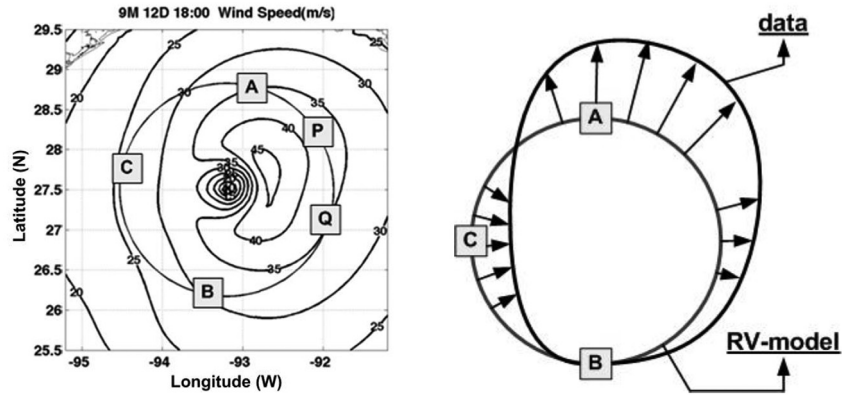
Fig. 8   Deformation schematic

Table 2   Deformation ratios

	Number of HWIND wind field data	$d_A = \left(\overline{V_A/V_B}\right)$	$d_B = \left(\overline{V_B/V_B}\right)$	$d_C = \left(\overline{V_C/V_B}\right)$
Ivan	12	1.114	1	0.842
Katrina	11	1.142	1	0.875
Rita	13	1.166	1	0.872
Dolly	7	1.180	1	0.703
Ike	13	1.160	1	0.838
Average		1.152	1	0.826
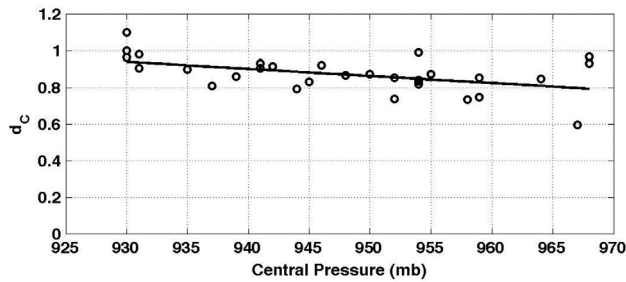
Fig. 9   Best-fit line for d_c vs P_c

For $V_m > 70$ m/s, the pattern is largely reversed and the data (Fig. 15) suggested using the following form

$$\frac{\Delta(r,\theta)}{\Delta_m(\theta)} = 4.868 e^{-5} r^4 - 0.001871 r^3 + 0.02643 r^2 - 0.02104 r + 0.115 \tag{12}$$

For 50 m/s $< V_m <$ 70 m/s, the discrepancy between the modeled wind speed and H*Wind was negligible for the most part.

Note that the left hand side of Eqs. (11) and (12) is a measure of $F_2(r)$ because

$$\frac{\Delta(r,\theta)}{\Delta_m(\theta)} = \frac{F_2(r) \cdot E(\theta)}{F_2(4R_m) \cdot E(\theta)} = \frac{F_2(r)}{F_2(4R_m)} \tag{13}$$

As a result of Eqs. (8) and (13), it may be seen that $E(\theta)$ would represent the normalized velocity discrepancies along a circle with $r = 4R_m$. To estimate $E(\theta)$, the discrepancy along this circle at $\theta = 0°$, 90°, 180°, and 270° were used. These four locations are denoted by A, B, C, and D, and the discrepancies at these locations are denoted by E^A, E^B, E^C, and E^D. A curve was fitted to the values at these four locations to estimate $E(\theta)$ for other values of θ, in a manner analogous to that for $d(\theta)$. An examination of the data showed that these normalized discrepancies at A, B, C, and D varied with V_m. As was the case for the radial error, the parameters showed different characteristics for large wind speeds ($V_m > 60$ m/s) and for moderate wind speeds (36 m/s $< V_m <$ 50 m/s). A detailed examination of the discrepancies led to the following expressions

$$E^B = 0.4(V_m - 70)/10, \quad \text{for} \quad V_m > 70$$
$$E^B = 0.9(50 - V_m)/20 \quad \text{for} \quad 36 < V_m < 50 \tag{14a}$$
$$E^B = 0, \quad \text{otherwise}$$

$$E^D = 0.5(V_m - 60)/20, \quad \text{for} \quad V_m > 60$$
$$E^D = 0.7(50 - V_m)/20, \quad \text{for} \quad 36 < V_m < 50 \tag{14b}$$
$$E^D = 0, \quad \text{otherwise}$$

In general, we found that $E^A \approx E^C \approx (E^B + E^D)/2$.

With these parameterizations, the function $E(\theta)$ was defined as $E(\theta) = a_1 \cos(2\theta) + b_1$ for $0 < \theta < \pi$ and $E(\theta) = a_2 \cos(2\theta)$
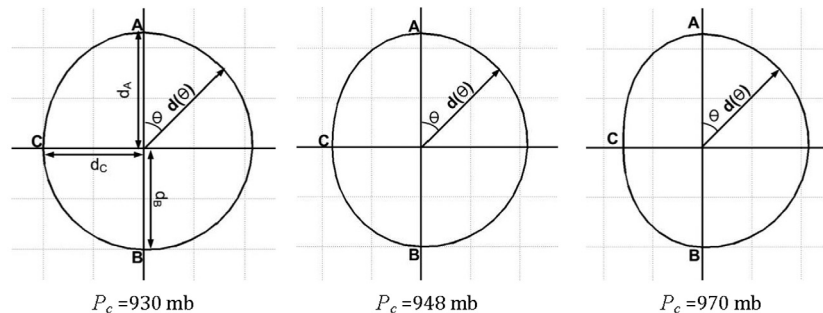

$P_c = 930$ mb $P_c = 948$ mb $P_c = 970$ mb

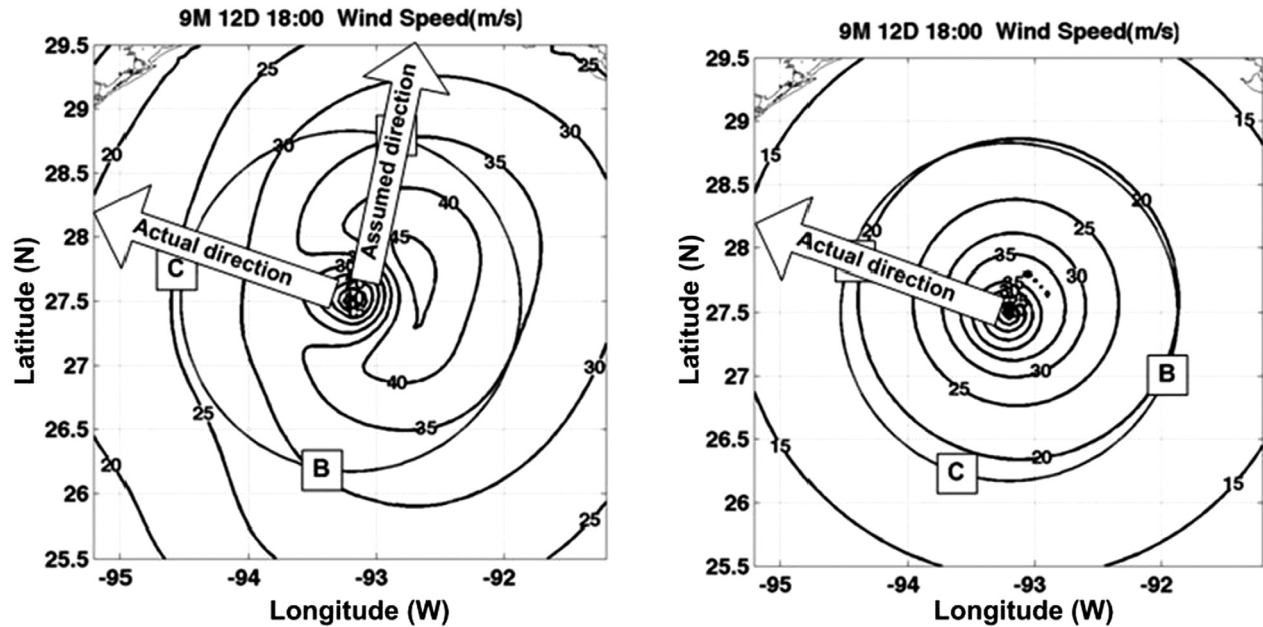**Fig. 10   The $d(\theta)$ for different central pressure**

Fig. 11 Wind speeds (m/s) during Hurricane Ike (2008, $\theta_d = 305°$): H*Wind (left), and RV-model (right)

Table 3 Storm direction dependence on central pressure and translation speed

Sector	P_c (mb)	V_s (m/s)	θ_c
$180 < \theta < 255$			-90
$255 < \theta < 285$		$V_s \leq 3.88$	90
		$V_s > 3.88$	$90 - 60 \cdot (1 - \gamma)$
$285 < \theta < 315$	$P_c \geq 970$	$V_s > 3.88$	$60 \cdot (1 - \gamma)$
	$P_c < 970$	$V_s \leq 3.88$	$60 \cdot \alpha$[a]
		$V_s > 3.88$	$60 \cdot \alpha + 60 \cdot (1 - \gamma)$
$315 < \theta < 340$	$P_c \geq 970$	$V_s > 3.88$	$60 \cdot (1 - \gamma)$
	$P_c < 970$	$V_s \leq 3.88$	$60 \cdot \alpha$
		$V_s > 3.88$	$60 \cdot (1 - \gamma)$
$340 < \theta < 360$		$V_s > 3.88$	$60 \cdot (1 - \gamma)/2$

Note: $\gamma = (5.55 - V_s)/1.67$ (for $3.88 \leq V_s \leq 5.55$), $\gamma = 0$ (for $V_s > 5.55$), and $\gamma = 1$ (for $V_s < 3.88$).
[a]α is defined in Eq. (6).

$+ b_2$ for $\pi < \theta < 2\pi$, where the constants a_1, a_2, b_1, and b_2 are determined from the conditions $E(\theta) = E^D$ at $\theta = 3/2\pi$ and $E(\theta) = E^B$ at $\theta = \pi/2$. The final form of $E(\theta)$ reduced to

$$E(\theta) = [(E^D - E^B) \cdot \cos 2\theta + (3E^B + E^D)]/4 \quad 0 < \theta < \pi \\ E(\theta) = [(E^B - E^D) \cdot \cos 2\theta + (E^B + 3E^D)]/4 \quad \pi < \theta < 2\pi \quad (15)$$

To conclude, a detailed examination of five storms (approximately 56 plots) suggested that the 10 m elevation wind could be obtained by adjusting the RV model as follows

$$V_{CRV} = V_{RV} \cdot d(\theta) \cdot C_B \quad (16)$$

The effect of this second adjustment may be seen in Figs. 12(e) and 12(f) for Hurricane Ike and in Fig. 16 for Hurricane Katrina. We note that in the case of Hurricane Katrina, the shape obtained by the original RV-model is reasonable, although for both storms, the final adjusted velocities based on eq. (15) are significantly improved as compared to the original RV model results. The effect of our modifications on the wave heights during Hurricane

Katrina is shown in Fig. 6; the differences are of a magnitude sufficient to influence extreme wave height calculations.

4 Validation and Effect on Wave Fields

As noted earlier, the Reanalysis wind fields are available on a 6-hourly basis, dating back to 1948, and have occasionally been used for wave and storm-surge hindcasting [16–20,37]. However, the coarse resolution ($2.5° \times 2.5°$) can be expected to adversely impact the wind and wave hindcasts in hurricane conditions. For example, considering the case of Hurricane Gordon, as mentioned in Sec. 1, winds resulting from the modified RV model are shown in Fig. 17. The wave hindcast resulting from these wind fields is compared with data from buoy 42 003 in Fig. 18. It is clear that the Reanalysis winds are inadequate for reliable wave height predictions and that the modified RV model results in better wave predictions, with a maximum difference on the order of 4 m.

Nonetheless, the Reanalysis winds can be used to provide the "background" windfields, viz., the windfields outside the hurricane and also the windfields that existed before the onset of the hurricane. The benefits of incorporating such background windfields have been indicated by Liu et al. [35]. We have, therefore, constructed a composite windfield dataset by merging the modified RV winds with the Reanalysis winds (the latter are interpolated onto a 5 km grid).

The parametric model equation (Eq. (16)) was tested against 17 storms (107 plots) covering a period from 1961 to 2008 (Table 4); these formed a subset of the entire H*Wind dataset. The others were not chosen because numerical data were not available for them or because they contained too many land points.

For each snapshot $V(x, y)$ was calculated using Eq. (15) for a matrix containing 81×81 points on each side (at a resolution of approximately 5 km) covering a $4° \times 4°$ region (approximately 6561 grid points per snapshot). Wind speeds from the modified RV model and the original RV models were compared with the H*Wind data for these grid points for each snapshot. The average of all of the absolute values of the percentage error at each grid point, denoted by AE, is presented in Table 5. In general, in 14 out of 17 cases, the modified RV model (V_{CRV}) produces far lower errors than the original model. Disregarding small differences (say, less than 10%, which occur in eight cases), eight of the
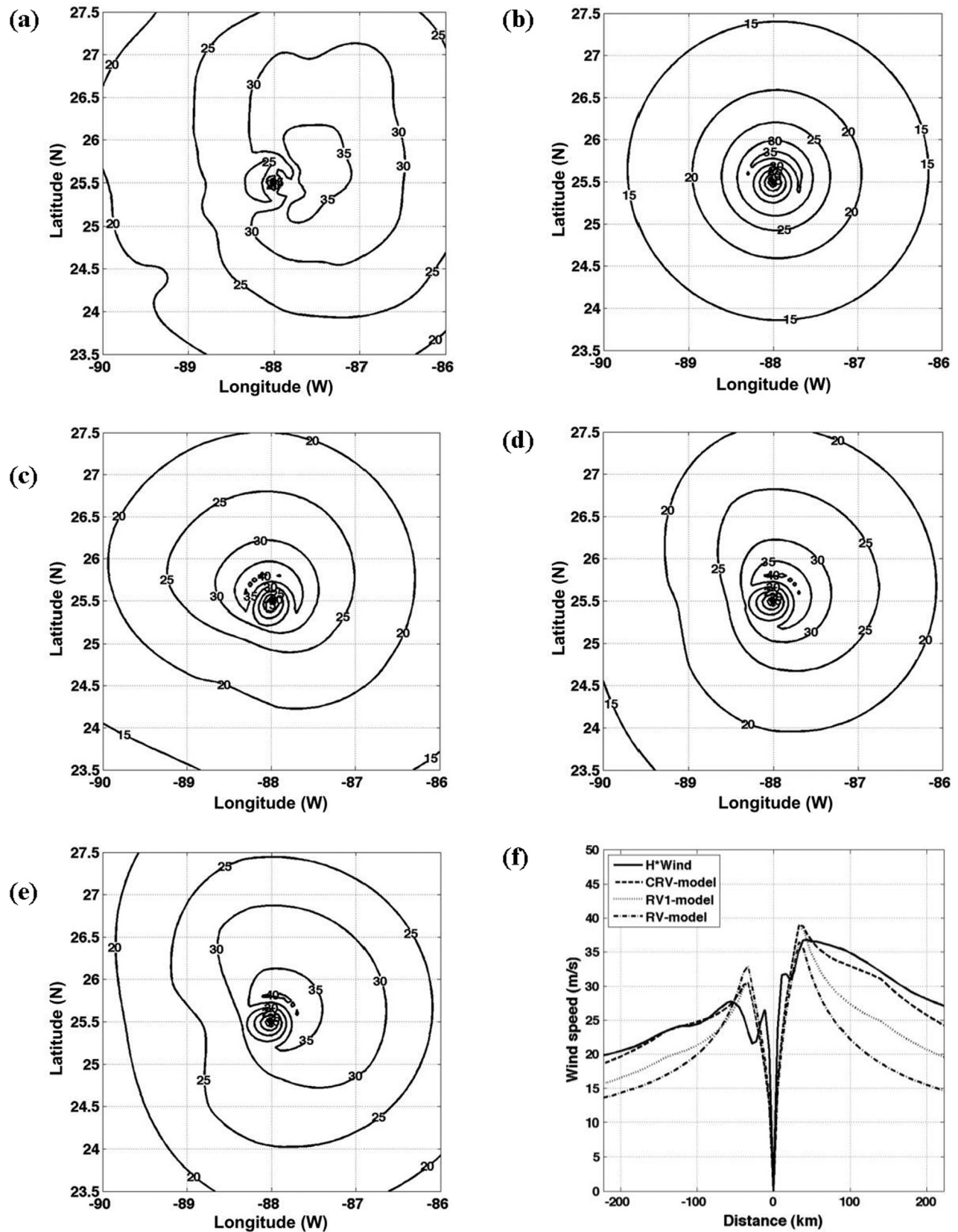
Fig. 12 Wind speeds (m/s) for Hurricane Ike at UTC 1200 11 Sept. 2008; $\theta_d = 295°$, $V_S = 4.44$ m/s, $P_c = 946$ mb (*a*) H*Wind, (*b*) RV-model, (*c*) before angle correction with $d(\theta)$, (*d*) after angle correction with $d(\theta)$, (*e*) after application of both correction factors, and (*f*) comparison along the central E-W transect
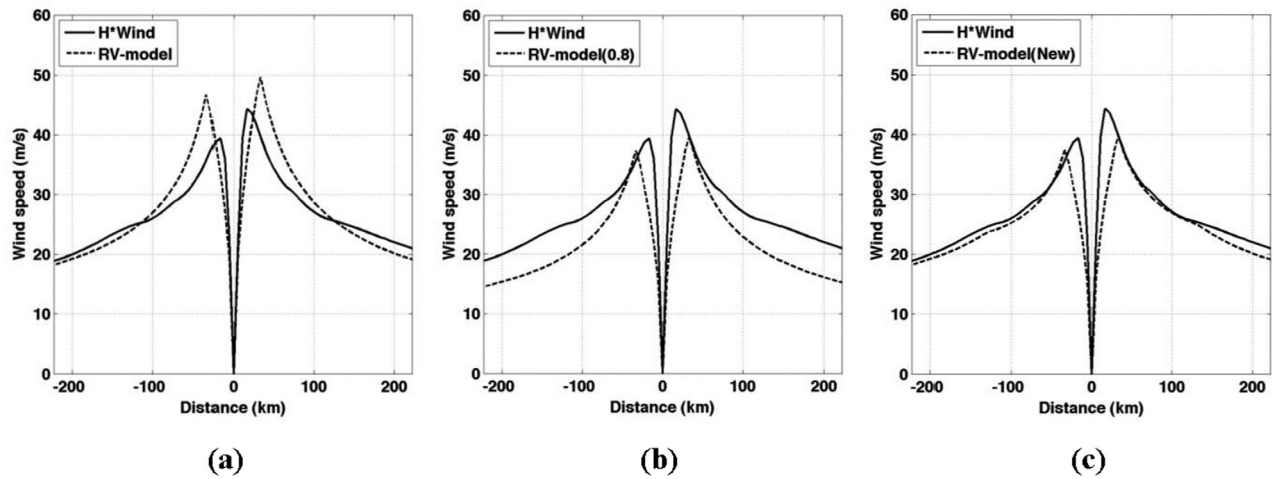
Fig. 13 Wind speed along the central transect for the (*a*) H*Wind and RV model, (*b*) H*Wind and RV-model with 10-meter elevation correction factor ($\cong 0.8$), and (*c*) H*Wind and RV-model with the 10-meter elevation correction factor (from Eq. (9))
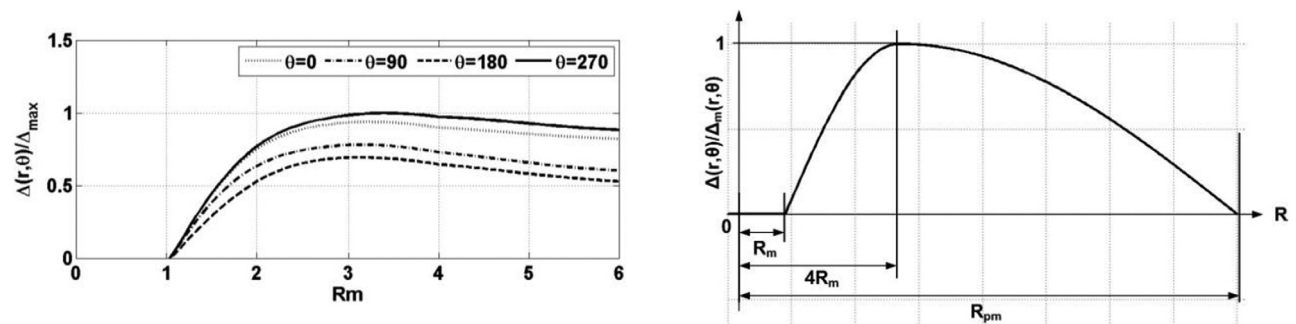
Fig. 14 Model-data discrepancies for Hurricane Ike: $V_m = 48.6$ m/s (left), and best-fit curve based on 400 data points (right)
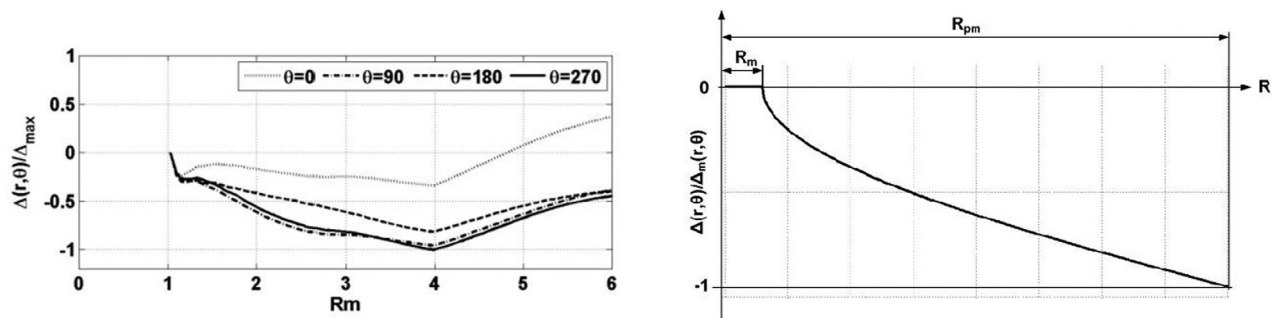

Fig. 15 Model-data discrepancies for Hurricane Rita with $V_m = 79.2$ m/s (left), and best-fit curve based on 400 data points (right)

remaining nine showed significant improvements, while only one (i.e., Hurricane Dennis) showed considerable deterioration relative to the original RV model. The maximum improvement is for Hurricane Dean (30%). Unfortunately, for the two cases with maximum discrepancies (i.e., Hurricanes Dennis and Dean), the assessment depends on very few snapshots being available. In addition, a detailed comparison of both parametric wind fields against the H*Wind data was conducted for Hurricane Georges (1998) and the results are in shown in Fig. 19.

The results indicate clearly that the CRV-model wind speed contour shape shows a better match with the H*Wind than the RV-model plot. The wave fields resulting from the two numerically generated wind fields are shown in Fig. 19 (bottom). For both wind and wave fields, although the maximum values are largely the same, the spatial patterns are different, leading to a maximum of about a ± 1.8 m difference in wave height estimates at some locations. A difference on the order of about 3.5 m in the maximum SWH is obtained for Hurricane Katrina (see Fig. 6
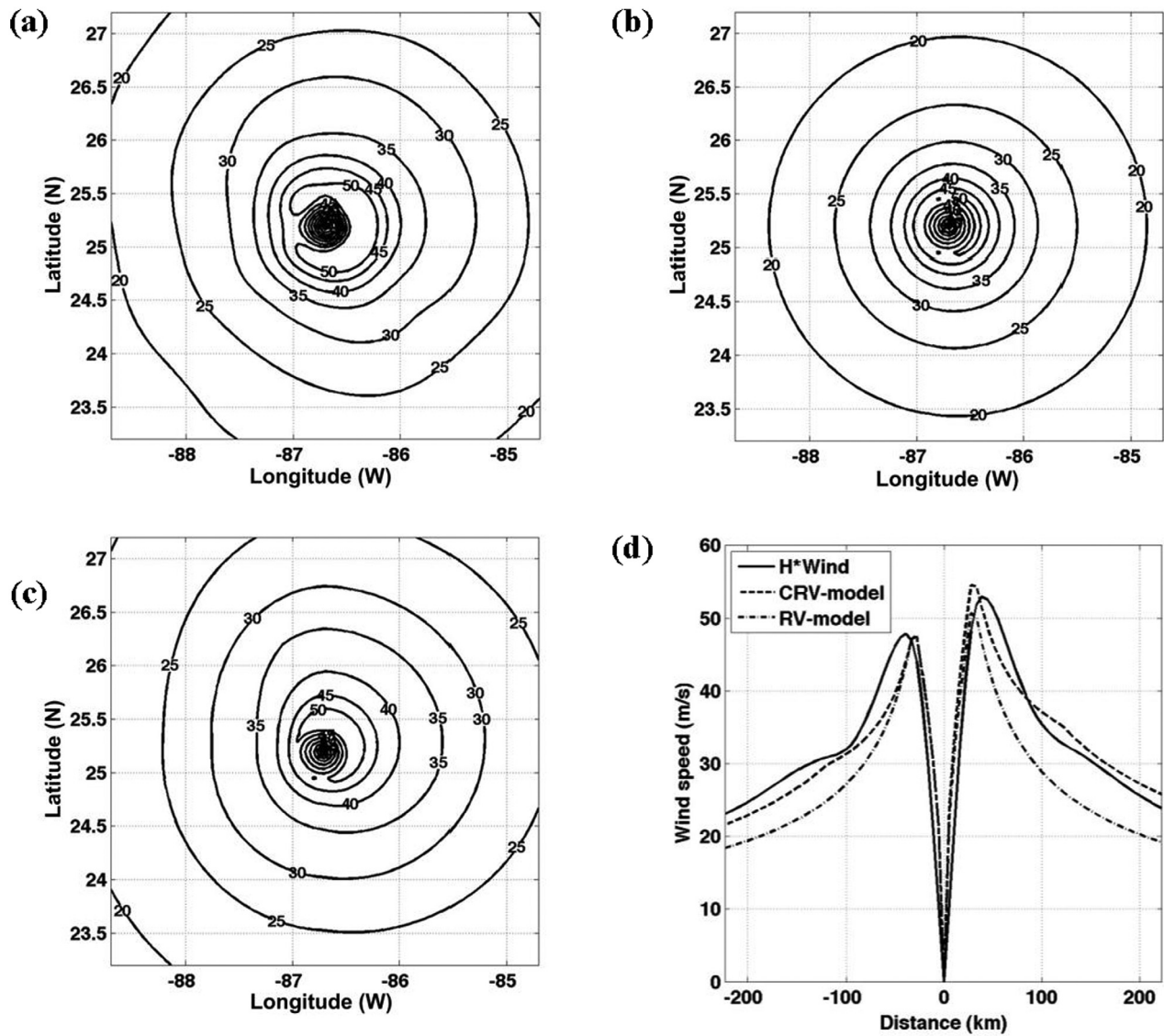
Fig. 16 Wind speeds (m/s) during Hurricane Katrina (0600 UTC 28 Aug. 2005); (*a*) H*Wind, (*b*) RV-model, (*c*) CRV-model, and (*d*) comparison along the central transect
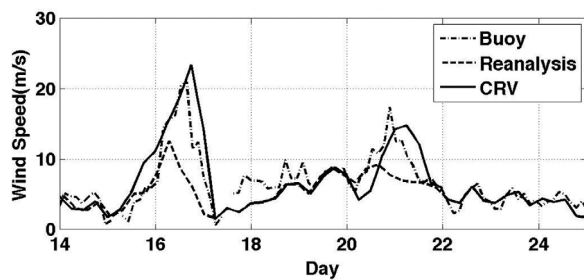

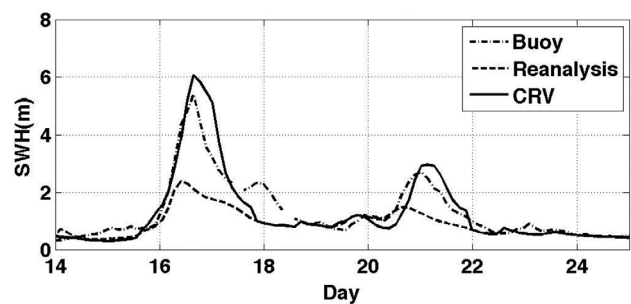**Fig. 17 Wind speed during Sept. 2000 at NDBC buoy 42 003**

Fig. 18 SWHs during Hurricane Gordon (Sept. 2000) at NDBC buoy 42 003 (located approximately 57 km from storm track)

where buoy data are also shown) and about 4 m for Hurricane Ike (not shown). Such large differences have the potential to affect the calculations of extreme wave statistics.

Finally, the effect of the two wind fields (V_{RV} and V_{CRV}) on the 100-yr return period SWHs (defined by SWH_{100}) are examined. These extreme wave height calculations were made by fitting the Gumbel distribution to 51 years of simulations (1958–2008). The purpose of this exercise was merely to study the differences;

actual estimates of SWH_{100} would depend on the type of statistical model used, and other factors which will be discussed in a separate paper. The results (Fig. 20) show considerable differences in the spatial patterns. These differences (on the order of 4 m at some locations; see Fig. 20(*c*)), are substantial relative to the SWH_{100} obtained using the original RV model and also relative to the values used by API (2000) [1].

Table 4 Hurricanes selected to test Eq. (16)

No.	Name	Storm period	Number of HWIND storm snapshots chosen
1	Carla (1961)	Sep. 03. 12:00–Sep. 16. 00:00	2
2	Georges (1998)	Sep. 15. 12:00–Oct. 01. 06:00	9
3	Gordon (2000)	Sep. 14. 12:00–Sep. 21. 06:00	5
4	Isidore (2002)	Sep. 14. 18:00–Sep. 27. 18:00	5
5	Lili (2002)	Sep. 21. 18:00–Oct. 04. 12:00	4
6	Ivan (2004)	Sep. 02. 18:00–Sep. 24. 06:00	12
7	Arlene (2005)	June 08. 18:00–June 14. 06:00	4
8	Dennis (2005)	July. 04. 18:00–July 18. 06:00	3
9	Emily (2005)	July 11. 00:00–July 21. 12:00	6
10	Katrina (2005)	Aug. 23. 18:00–Aug. 31. 06:00	9
11	Rita (2005)	Sep. 18. 00:00–Sep. 26. 06:00	10
12	Wilma (2005)	Oct. 15. 18:00–Oct. 26. 18:00	12
13	Alberto (2006)	June 10. 06:00–June 19. 06:00	3
14	Dean (2007)	Aug. 13. 06:00–Aug. 23. 00:00	2
15	Dolly (2008)	July 20. 12:00–July 27. 00:00	4
16	Gustav (2008)	Aug. 25. 00:00–Sep. 05. 12:00	5
17	Ike (2008)	Sep. 01. 06:00–Sep. 15. 12:00	12

Table 5 Performance of RV and CRV models

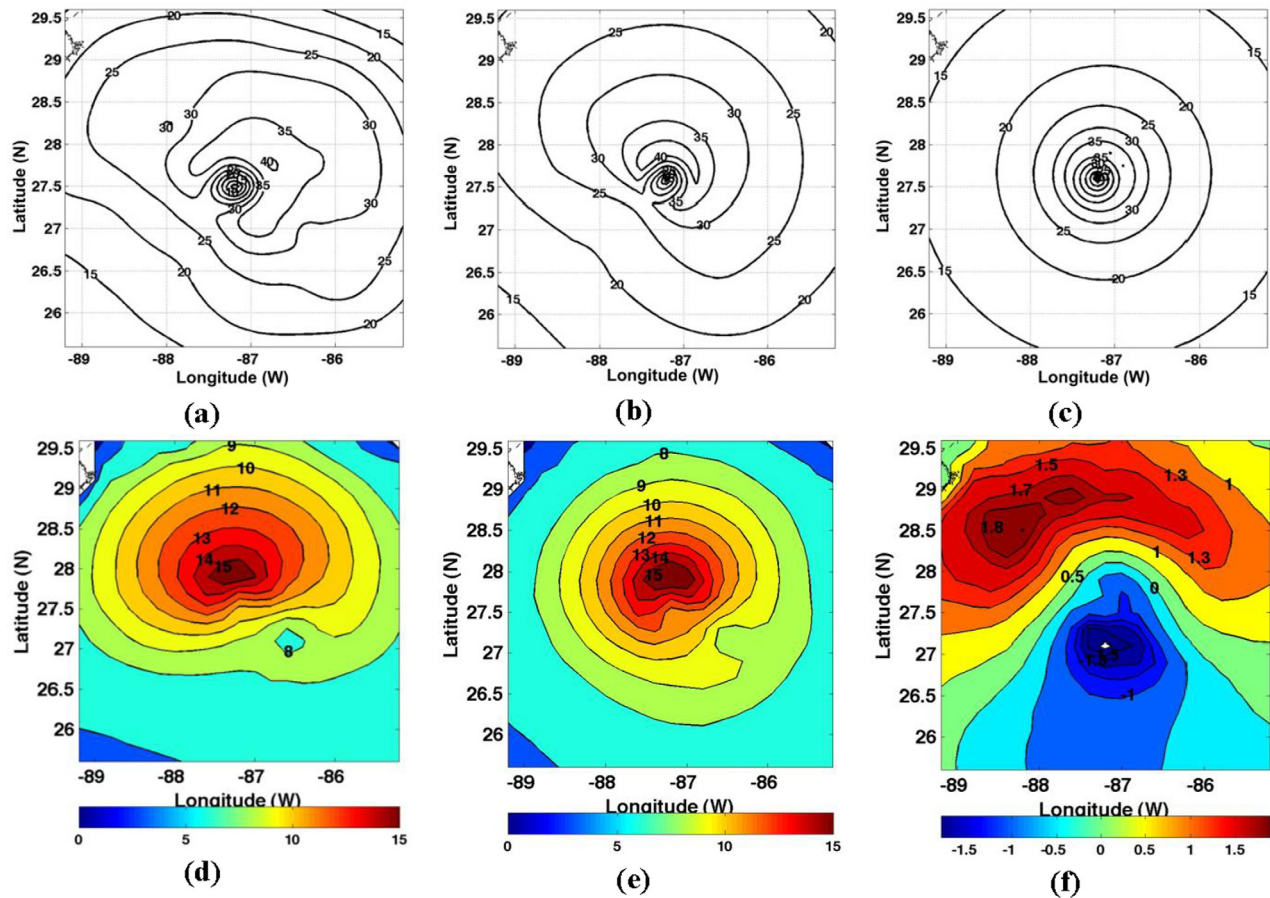| No.	Hurricane	N	AE (CRV model) (%)	AE (RV model) (%)
1	Carla	2	15	20
2	Georges	9	12	26
3	Gordon	5	22	26
4	Isidore	5	37	45
5	Lili	4	23	16
6	Ivan	12	11	24
7	Arlene	4	32	34
8	Dennis	3	38	20
9	Emily	6	26	20
10	Katrina	9	9	20
11	Rita	10	10	16
12	Wilma	12	11	30
13	Alberto	3	19	24
14	Dean	2	12	42
15	Dolly	4	20	33
16	Gustav	5	8	22
17	Ike	12	14	39

Fig. 19 Wind speeds (m/s) and SWHs during Hurricane Georges (at 0600 UTC 27 Sept. 1998): (a) H*Wind, (b) CRV-model wind, (c) RV-model wind, (d) SWH (m) using CRV-model wind, (e) SWH (m) using RV-model wind, and (f) the difference SWH (m) between (d) and (e)

5 Conclusions

An integrated set of offshore and coastal models for winds, tides, waves, and storms (hurricanes and typhoons) is extremely useful in the planning and in the management of an emergency response pertaining to tropical storms that affect US coasts and islands. These models are also used in other areas of coastal engineering concerned with the design of coastal and wetland protection systems such as barrier islands, levees, and coastal navigation and harbor structures. In these applications, users need models with varying complexity and accuracy for calculating winds when modeling past storm events (hindcast), future storms (forecast), and hypothetical (synthetic) storms. Less resource-demanding models that run fast with a low-order accuracy may be used to perform quick simulations for decision-making and to determine if further modeling using models of higher accuracy is warranted.
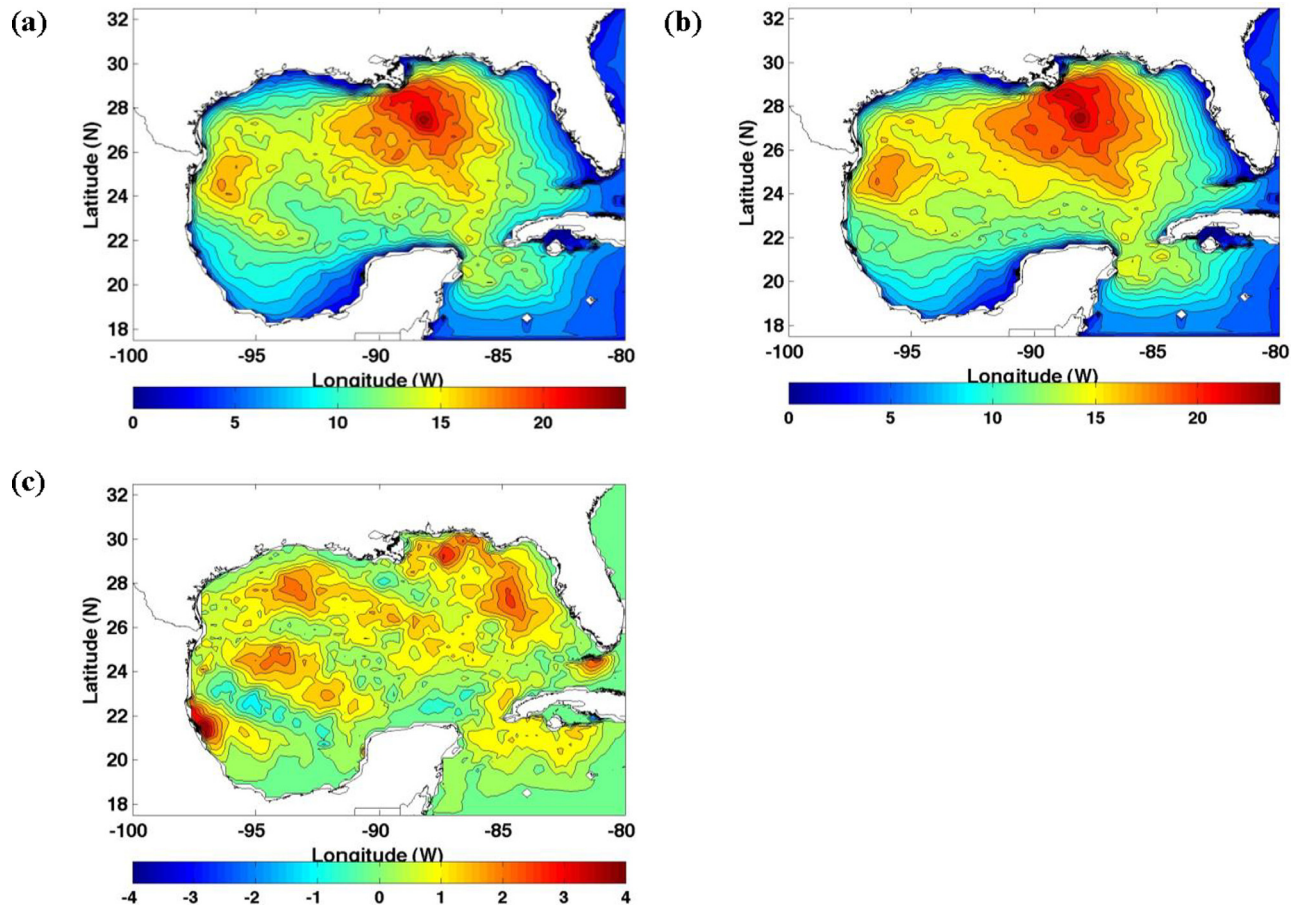
Fig. 20 SWH$_{100}$ (m) for the Gulf of Mexico estimated using (*a*) RV-model wind, (*b*) CRV-model wind, and (*c*) differences between (*a*) and (*b*)

The parametric wind modeling approach described in this paper is intended to address these critical needs, which can be used to estimate winds when no other information is available for historical storms of interest.

We have investigated the RV model and other similar recent parametric wind models with corrections for a large number of tropical storms in the GOM. We found that these models produced a substantial difference in wind speeds relative to the H*Wind data in the GOM. This motivated us to consider spatial adjustments to the shape and distributions to the contours produced by the RV model. We developed an adjusted model (CRV) applicable to asymmetric wind fields typically observed in tropical storms, and have conducted a thorough testing of it against H*Wind for several hurricanes.

The CRV model, for the most part, produced a better shape and distribution of the velocity plots. In a comparison performed for 17 hurricanes with 56 snapshots, the CRV model produced smaller percentage errors than the RV model. The CRV wind fields produced SWHs which were on the order of 4 m higher for some hurricanes examined. Results presented in Figs. 6 and 18 show a better match with data. The estimates of SWH$_{100}$ resulted in a 4-m difference (maximum) at some locations.

Acknowledgment

References

[1] American Petroleum Institute, 2000, "Recommended Practice for Planning, Designing and Constructing Fixed Offshore Platforms—Working Stress Design," API Recommended Practice No. 2A-WSD.

[2] American Petroleum Institute, 2007, "Interim Guidance on Hurricane Conditions in the Gulf of Mexico," API Bulletin No. 2INT-MET.

[3] Palao, I. M., Teng, C. C., and Brown, D. A., 1994, "An Extremal Analysis of Significant Wave Height Data Measured From NDBC Buoys", Report No. 1804–07.01, NDBC, Stennis Space Center, MS, USA.

[4] Panchang, V. G., Zhao, L., and Demirbilek, Z., 1999, "Estimation of Extreme Wave Heights Using GEOSAT Measurements," Ocean Eng., **26**, pp. 205–225.

[5] Jeong and Panchang, 2008, "Measurement-based Estimates of Extreme Wave Conditions for the Gulf of Mexico," MTS/IEEE Oceans 2008 Conference, Quebec, Canada.

[6] Panchang, V. G. and Li, D., 2006, "Large Waves in the Gulf of Mexico Caused by Hurricane Ivan," Bull. Am. Meteorol. Soc., **87**(4), pp. 481–489.

[7] Berek, E. P., Cooper, C. K., Driver, D. B., Heideman, J. C., Mitchell, D. A., Stear, J. D., and Vogel, M. J., 2007, "Development of Revised Gulf of Mexico Metocean Hurricane Conditions for Reference by API Recommended Practices," Offshore Technology Conference, Houston.

[8] Goo, J., Demirbilek, Z., Smith, J., and Sanchez, A., 2010, "TWAVE Users Guide With Example Application to Oahu, Hawaii," Coastal and Hydraulics Laboratory Technical Report Technical Note No. ERDC/CHL CHETN-I-81, Vicksburg, MS.

[9] Sanchez, A., Demirbilek, Z., and Smith, J., 2009, "TWAVE: A Modeling System for Flooding and inundation of Islands by Tropical Storms," Coastal and Hydraulics Laboratory Technical Report No. ERDC/CHL TR-09–2, Vicksburg, MS.

[10] Sanchez, A., Smith, J., Demirbilek, Z., and Boc, S., 2007, "Combined Wind and Waves Over a Reef," Proceedings of the 10th International Workshop, Wave Hindcasting and Forecasting and Coastal Hazard Symposium, Oahu, HI.

[11] Thompson, E. F. and Scheffner N. W., 2002, "Typhoon-Induced Stage-Frequency and Overtopping Relationship for the Commercial Port Road, Territory of Guam," Coastal and Hydraulics Laboratory Technical Report No. ERDC/CHL TR-02–01, Vicksburg, MS.

[12] Thompson, E. F. and Cardone., V. J., 1996, "Practical Modeling of Hurricane Surface Wind Fields," ASCE J. Waterway, Port, Coastal, Ocean Eng., **122**(4), pp. 195–205.

[13] Demirbilek, Z., Nwogu, O. G., Ward, D. L., and Sanchez, A., 2009, "Wave Transformation Over Reefs: Evaluation of One-Dimensional Numerical

Models," Coastal and Hydraulics Laboratory Technical Report No. ERDC/CHL TR-09–1, Vicksburg, MS.

[14] Demirbilek, Z. and Nwogu, O. G., 2007, "Boussinesq Modeling of Wave Propagation and Runup Over Fringing Coral Reefs, Model Evaluation Report," Coastal and Hydraulics Laboratory Technical Report No. ERDC/CHL-TR-07-12, Vicksburg, MS.

[15] Kalnay, E., Kanamitsu, M., Kistler, R., Collins, W., Deaven, D., Gandin, L., Iredell, M., Saha, S., White, G., Woollen, J., Zhu, Y., Leetmaa, A., Reynolds, R., Chelliah, M., Ebisuzaki, W., Higgins, W., Janowiak, J., Mo, K. C., Ropelewski, C., Wang, J., Jenne, E., and Joseph, D., 1995, "The NCEP/NCAR 40-Year Reanalysis Project," Bull. Am. Meteorol. Soc., **77**, pp. 437–471.

[16] Music, S. and Nickovic, S., 2008, "44-Year Wave Hindcast for the Eastern Mediterranean," Coastal Eng., **55**, pp. 872–880.

[17] Cieœlikiewicz, W., and Paplińska-Swerpel, B., 2008, "A 44-year Hindcast of Wind Wave Fields Over the Baltic Sea," Coastal Eng., **55**, pp. 894–905.

[18] Pilar, P., Soares, C. G., Carretero, J. C., 2008, "44-Year Wave Hindcast for the North East Atlantic European Coast," Coastal Eng., **55**, pp. 861–871.

[19] Wang, X. L. and Swail, V. R., 2002, "Trends of Atlantic Wave Extremes as Simulated in a 40-Year Wave Hindcast Using Kinematically Reanalyzed Wind Fields," J. Climate, **15**, pp. 1020–1035.

[20] Wang, X. L., Zwiers, F. W., and Swail, V. R., 2004, "North Atlantic Ocean Wave Climate Change Scenarios for the Twenty-First Century," J. Climate, **17**(12), pp. 2368–2383.

[21] Powell, M. D., and Houston, S. H., 1996, "Hurricane Andrew's Landfall in South Florida. Part II: Surface Wind Fields and Potential Real-Time Applications," Weather Forecast., **11**, pp. 329–349.

[22] Powell, M. D., Houston, S. H., Amat, L. R., and Morisseau-Leroy, N., 1998, "The HRD Real-Time Surface Wind Analysis System," J. Wind Eng. Ind. Aerodyn., **77/78**, pp. 53–64.

[23] Kennedy, A., Rogers, S., Sallager, A., Gravois, U., Zachry, B., Dosa, M., and Zarama, F., 2011, "Building Destruction From Wave and Surge on the Bolivar Peninsula During Hurricane Ike," J. Waterway, Port, Coastal, Ocean Eng., **137**, p. 132.

[24] Powell, M. D., Murillo, S., Dodge, P., and Uhlhorn, E., 2010, "Reconstruction of Hurricane Katrina's Wind Fields for Storm Surge and Water Hindcasting," Ocean Eng., **37**, pp. 26–36.

[25] Phadke, A. C., Martino, C. D., Cheung, K. F., and Houston, S. H., 2003, "Modeling of Tropical Cyclone Winds and Waves for Emergency Management," Ocean Eng., **30**, pp. 553–578.

[26] MacAfee, A. W. and Pearson, G. M., 2006, "Development and Testing of Tropical Cyclone Parametric Wind Models Tailored for Midlatitude Application—Preliminary Results," Appl. Meteorol. Climatol., **45**, pp. 1244–1260.

[27] Xie, L., Bao, S., Pietrafesa, L. J., Foley, K., and Fuentes, M., 2006, "A Real-Time Hurricane Surface Wind Forecasting Model: Formulation and Verification," Mon. Weather Rev., **134**, pp. 1355–1370.

[28] Houston, S. H., and Powell, M. D., 1994, "Observed and Modeled Wind and Water-Level Response From Tropical Storm Marco (1990)," Weather Forecast., **9**, pp. 427–439.

[29] Holland G. J., 1980, "An Analytic Model of the Wind and Pressure Profiles in Hurricanes," Mon. Weather Rev., **108**, pp. 1212–1218.

[30] DeMaria, M., Aberson, S., Ooyama, K. V., and S. J. Lord, S. J., 1992, "A Nested Spectral Model for Hurricane Track Forecasting," Mon. Weather Rev., **120**, pp. 1628–1643.

[31] Willoughby, H. E. and Rahn, M. E., 2002, "A New Parametric Model of Hurricane Wind Profiles," 25th Conference on Hurricanes and Tropical Meteorology, San Diego, preprints pp. 553–554.

[32] Emanuel, K., Rarela, S., Vivant, E., and Risi, C., 2006, "A Statistical Approach to Hurricane Risk Assessment," Bull. Am. Meteorol. Soc., **87**, pp. 290–314.

[33] Georgiou, P., 1985, "Design Wind Speeds in Tropical Cyclone Prone Regions," Ph.D. thesis, University of Western Ontario, London, Ontario, Canada, p. 295.

[34] Willoughby, H. E., Darling, E. R., and Rahn, M. E., 2006, "Parametric Representation of the Primary Hurricane Vortex, Part II: A New Family of Sectionally Continuous Profiles," Mon. Weather Rev., **134**, pp. 1102–1120.

[35] Liu, H., Xie, L., Pietrafesa, L. J., and Bao, S., 2007, "Sensitivity of Wind Waves to Hurricane Wind Characteristics," Ocean Modell., **18**, pp. 37–52.

[36] Bretschneider, C. L., 1972, "A Non-Dimensional Stationary Hurricane Wave Model," Offshore Technology Conference, I, pp. 55–68.

[37] Sebastião, P., Soares, C. G., and Alvarez, E., 2008, "44 Years Hindcast of Sea Level in the Atlantic Coast of Europe," Coastal Eng., **55**, pp. 843–848.